Preparation and properties of carbon nanotubes with deposited bimetal oxide nanoparticles

L. B. OKHLOPKOVA, O. S. EFIMOVA, L. M. KHITSOVA, Z. R. ISMAGILOV

Federal Research Center of Coal and Coal Chemistry, Siberian Branch of the Russian Academy of Sciences, Kemerovo, Russia

E-mail: lokhlopkova@yandex.ru

Abstract

In order to develop new catalysts based on carbon nanotubes (Taunite) with deposited bimetallic oxide nanoparticles for oxidative desulphurization, a series of samples with the composition $M_1M_2O_x$/Taunite (M_1M_2 = CeMo, CuMo, CeCu) was prepared by incipient wetness impregnation. The properties of the catalysts were studied by means of FTIR spectroscopy and thermal analysis combined with mass spectrometry. The effects of the nature of a metal precursor and the oxidative treatment of the support on the functionalization of the support surface and support thermal stability were studied. Decomposition of supports with deposited bimetals was determined to start at a temperature lower by 210–285 °C than in the case of non-modified support. The stability of Taunite support against thermal decomposition increases in the following series of metal cations: CuMo < CeMo < CeCu < support without M_1M_2. The optimal precursors of bimetals for the synthesis of a promising nanosized catalyst $M_1M_2O_x$/Taunite were selected.

Keywords: carbon nanomaterial, bimetallic oxide nanoparticles, catalyst, thermal analysis, FTIR spectroscopy

INTRODUCTION

Organosulphur compounds are known to be present in crude oil and remain in the liquid fuel after petroleum processing. The combustion of fuel inevitably leads to the formation of a large amount of sulphur oxides (SO_x), which is one of the basic reasons for acid rain. Because of this, the desulphurization of liquid fuel attracts special attention of researchers all over the world. At present, hydrodesulphurization (reductive desulphurization, RDS) is a widely used industrial method to remove sulphur-containing compounds. However, RDS has many disadvantages: high process temperatures (320–380 °C) and high hydrogen pressure (30–70 atm), as well as low efficiency of the removal of aromatic sulphur-containing compounds with a high melting point, for example, dibenzothiophene (DBT) and its derivatives. Much attention is paid to oxidative desulphurization (ODS) because the highly efficient removal of aromatic sulphur-containing compounds is carried out under soft conditions.

During recent decades, carbon materials such as graphitized carbon and carbon nanotubes (CNT) have won broad application due to their low cost, high availability, sufficient chemical stability, unique optical and electrical characteristics. These nanomaterials are strongly hydrophobic, they can be readily mixed with model oil and may be used as ODS catalyst supports [1–3]. Carbon nanotubes provide high catalytic parameters due to good electronic conductance, which is necessary for electron transfer in the oxidation-reduction reaction, and the presence of carbonyl groups and surface defects. Microporosity and chemical composition of the surface are essential for efficient desulphurization, so different modifications of carbon materials are used to improve their texture characteristics [4].

Oxidation of the surface and inclusion of metals into the support lead to π-electron interactions

of sulphur-containing aromatic compounds with metals of carbon support [5], which has a positive influence on the efficiency of DBT adsorption [6]. On the one hand, the introduction of nanoparticles of transition metals with high electron mobility promotes an increase in catalytic activity [7]. On the other hand, the functional composition of the surface and the stability of carbon support to decomposition may be altered in the presence of metal-containing compounds [8]. A broad range of the oxides of transition metals, such as cerium, molybdenum and copper [9], are used as catalytically active phases in oxidative desulphurization. In spite of the efficiency of monometallic catalysts, it is confirmed that bimetal catalysts provide higher catalytic activity in ODS [5, 10−14]. For instance, it was assumed in [15] that the synergism of the Ce−Mo−O catalyst is due to oxygen activation on the surface of Ce particles and the formation of active oxygen forms, which provided additional oxidation of DBT on Mo-containing centres. At present, the efforts of researchers are mainly focused on the search for new systems based on bimetal supported oxides, however, the problem concerning their optimal composition, content and particle size remains unsolved. So, it is necessary to choose a corresponding metal precursor to carry out the successful synthesis of CNT with supported nanoparticles of bimetal oxides.

The goal of the work was to carry out IR Fourier spectroscopic investigation of the composition of functional groups on the surface of $M_1M_2O_x/$ Taunite samples (M_1M_2 = CeMo, CuMo, CeCu) prepared by means of incipient wetness impregnation, and to study the effect of metal precursor on the thermal stability of Taunite support.

EXPERIMENTAL

Materials

CNT Taunite (LC NanoTekhTsentr, Russia) was used as the support. Carbon nanotubes were multilayer nanostructured filament-like graphite in the form of tubes with an inner diameter of 10−20 nm and a specific surface area of 180 m^2/g. Physicochemical characteristics of the support were reported in [4]. The initial CNT sample was dried in a vacuum furnace at 13 mbar and 80 °C for 2 h. The sample was designated as Taunite.

CNT oxidation was carried out using concentrated nitric acid (HNO_3). CNT sample was wetted with distilled water, and the indicated amount of the acid was poured in. The mass ratio CNT/

liquid phase was 1 : 10. Then the temperature was increased to 85 °C, and the sample was kept at this temperature for 1 h under permanent mixing. After cooling to room temperature, the suspension of CNT was 5-fold diluted with distilled water, precipitated and centrifuged. The precipitate was washed with hot water several times (the mass ratio H_2O/CNT = 50 : 1) to obtain the neutral medium in rinsing water. After the oxidation procedure, the samples were dried in a vacuum furnace at 13 mbar and 80 °C for 4 h. The sample treated with HNO_3 is designated as Taunite-1.

The catalysts $M_1M_2O_x$/Taunite were obtained by means of incipient wetness impregnation of the support with the solutions of precursors of active metals. The salt $Ce(NO_3)_3 \cdot 6H_2O$ (Kh. Ch. − chemically pure reagent grade) was used as a precursor of cerium, $Cu(NO_3)_2 \cdot 3H_2O$ (Kh. Ch. reagent grade) − as a precursor of copper, $(NH_4)_6Mo_7O_{24} \cdot 4H_2O$ (Kh. Ch. reagent grade) − as a precursor of molybdenum. After impregnation, the samples were dried in vacuum at 13 mbar and 80 °C for 2 h to study them by means of thermal analysis (TA), then the samples were annealed in nitrogen flow (10 ml/min) at 600 °C for 2 h to carry out the analysis by means of IR Fourier spectroscopy. Metal content was constant (10 mass %). If not otherwise stated, the metal molar ratio was M_1/M_2 = 1 : 1.

Methods

The investigation by means of thermogravimetry (TG), differential thermogravimetry (DTG) and differential scanning calorimetry (DSC) was carried out with the help of an STA 449 F3 Jupiter thermal analyzer (NETZSCH, Germany). A portion of 8 mg was heated in a platinum crucible from 25 to 1000 °C in the atmosphere of N_2 at a rate of 5 °C/min. The apparatus for thermal analysis was connected in the online mode to the QMS 403 C Aëolos mass spectrometer (NETZSCH, Germany) to carry out parallel analysis of gaseous products by means of mass spectrometry (MS). The energy of the ion source was 80 eV. Ion currents were measured with the help of a CH-TRON detector for m/z (m is the molecular mass of a particle, z is its charge). The chosen m/z values correspond to the molecular and fragmentation ions that can be formed during the decomposition of the metal precursor and Taunite support. The intensity of ion peaks was calculated taking into account the background intensity.

The content of carbon, hydrogen, nitrogen and sulphur was measured using a Thermo Flash 2000 analyzer (Thermo Scientific, USA) by means of high-temperature catalytic oxidation of the samples in the reactor filled with CuO/Cu at a temperature of 1000 °C. Element content was determined in three parallel measurements.

The Fourier-transform infrared (FTIR) spectra were recorded with an Infralyum FT-08 instrument (GK Lyumeks, Russia) in a mixture of the sample with KBr (mass ratio 1 : 130). A mixture of CNT with KBr was mixed in a vibromill for 3 min to obtain a homogeneous substance. Then the mixture was pressed into a tablet under a pressure of 20 MPa. IR Fourier spectra were recorded within the range of 350–4000 cm^{-1} using 256 scans.

RESULTS AND DISCUSSION

FTIR spectroscopy

The FTIR spectra of Taunite, CuMo/Taunite, CeCu/Taunite, CeMo/Taunite (Fig. 1) are characterized by a broad set of absorption bands (a. b.) within the range 400–3500 cm^{-1}; some of them are caused by the vibrations of atoms in the lattice and the functional groups of carbon material, while the other (within the region 470–930 cm^{-1}) are due to vibrations in the supported components (CeO$_2$, CuO, MoO$_3$). In addition, the spectra contain a. b. in the region 3000–3580 cm^{-1}, which is connected with the stretching vibrations of water.

It should be stressed that the spectra of all samples contain broad a. b. at 1568 and 1584 cm^{-1}, which were attributed in [16] to vibrations with $E1u$ symmetry in the crystal structures of graphite. There are also a. b. at 2960, 2920 and 2850 cm^{-1} in the spectra. The former two bands correspond to asymmetric and symmetric stretching vibrations of CH$_3$ groups, while the band at 2850 cm^{-1} is due to the symmetrical stretching vibrations of the CH$_2$ group [17]. Bending vibrations of C–H bonds in CH$_2$/CH$_3$ groups (usually at 1370–1450 cm^{-1} [2]) appear in the spectrum of the sample as a band at 1431, 1404 or 1458 cm^{-1}. The bands at 1385 cm^{-1} correspond to the stretching vibrations of C–C bonds in the terminal alkyl
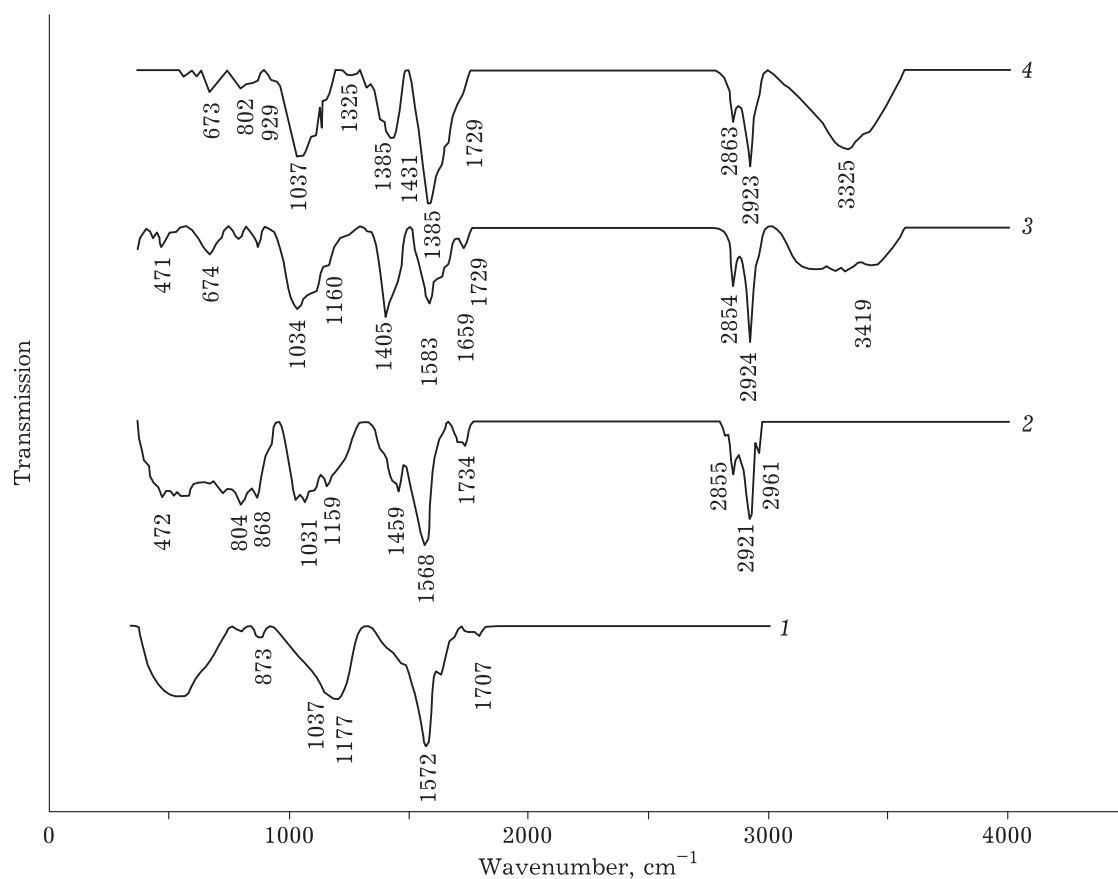
Fig. 1. FTIR spectra of samples: Taunite (*1*), CuMo/Taunite (*2*), CeCu/Taunite (*3*), CeMo/Taunite (*4*).

groups. In addition, the spectrum of Cu-Mo/Taunite contains a shoulder in the region of 2960 cm^{-1}, pointing to the presence of CH_3 groups. It was demonstrated in the studies of carbon nanofibres with different positions of graphite layers [18, 19] that defects in graphite structure are responsible for the bands appearing at 2947, 2917 and 2846 cm^{-1}, which are connected with the symmetrical stretching vibration of C−H bonds in CH_2/CH_3 groups.

The spectra of CuMo/Taunite, CeCu/Taunite and CeMo/Taunite samples also contain the a. b. with the maxima at 1707 and 1730 cm^{-1}. The bands within 1700−1740 and 1690−1655 cm^{-1} may be related to the stretching vibrations of C=O bonds in carboxylic (−COOH) and quinone groups [17, 19, 20], respectively. In this situation, the bands in the region of 1404−1458 cm^{-1} may be caused not only by bending vibrations of CH_2/CH_3 groups and the defects of graphite structures but also by a combination of the bending vibrations of C−O and C−H bonds in carboxylic groups [2]. It should be stressed that monomeric −COOH groups, unlike C−H groups, have a. b. in the region of 1190−1075 cm^{-1}, corresponding to C=O vibrations [17]. In our study, they may be observed as a shoulder at about 1075 cm^{-1} and a peak at 1159 cm^{-1} in CuMo/Taunite and CeCu/Taunite samples. In addition, the band at 1385 cm^{-1} may correspond to the vibrations of N=O in NO_2, for which the symmetrical and asymmetrical bands are in the regions of 1370−1390 and 1550−1580 cm^{-1}, respectively. Nitrogen content, estimated with the help of elemental analysis, is higher for Cu-containing samples and increases with an increase in Cu content (Table 1). Other a. b. at 1030 and 870 cm^{-1} may correspond to the stretching vibrations of ether bonds (C−O) and vinyl group (C−H) [21]. The band at 802 cm^{-1} may be attributed to the stretching vibrations of Mo−O−Mo bonds, while a shoulder at 929 cm^{-1} belongs to the stretching vibrations of Mo=O bonds [22]. The band at 674 cm^{-1} is likely to be connected with the stretching vibrations of Ce−O bonds [23], while the a. b. at 471 cm^{-1} relates to the stretching vibrations of Cu−O bonds (the phonon spectrum of CuO) [24]. The analysis of the spectra showed that the ratio of the intensities of a. b. at 1720 and 1190 cm^{-1} depends on the oxidative treatment of the Taunite sample. In Taunite-1, the indicated bands had maximal intensity (Fig. 2). The intensities of a. b. of CeCu/Taunite-1 and CeCu/Taunite samples are substantially lower than those of Taunite-1 but comparable with each other (see Fig. 2). Acid treatment leads to the oxidation of the surface of the Taunite sample and to an increase in the content of oxygenated groups, while surface decoration with Ce-Cu oxides decreases the concentration of oxygenated groups, which may be the evidence of the decomposition of the support in the presence of metal salts and/or the rupture of C=O bonds with the detachment of oxygen as a result of adsorption of the precursors.

Thermal analysis in combination with mass spectrometry

The TA and MS data for the support (CNT Taunite) are presented in Fig. 3, *a*. One can see that the Taunite sample is stable under thermal treatment in the inert atmosphere up to 500 °C. Between 500 and 1000 °C, mass loss (5.6 %) occurs due to sublimation of surface oxygen-containing functional groups. According to MS results, the major gaseous product is CO_2. Mass loss is not accompanied by thermal effects. So, Taunite may be used as a support for metal oxides to prepare $M_1M_2O_x$/Taunite catalysts containing CNT modified with nanoparticles. The TA and MS data for all precursors and samples of CNT with supported precursors are presented in Table 2.

It was demonstrated according to the TA data [9] that decomposition of the bulk compound $(NH_4)_6Mo_7O_{24} \cdot 4H_2O$ includes five stages with T_{DTA} = 95, 120, 200, 295 and 380 °C. Decomposition of bulk $Ce(NO_3)_3 \cdot 6H_2O$ proceeds in three stages, including two-stage dehydration process, the formation of anhydrous cerium nitrate, and the oxidation of Ce(III) by nitrate ion with the formation of CeO_2, and is characterized by mass losses at T_{DTG} = 95, 195 and 240 °C. Decomposition of the precursors of active component deposited on Taunite − $Ce(NO_3)_3 \cdot 6H_2O$ and $(NH_4)_6Mo_7O_{24} \cdot 4H_2O$ − proceeds in three stages (see Fig. 3, *b*). Three peaks on the DTG curve, accompanied by pronounced endothermic effects, are observed at T_{DTG} = 77, 181 and 221 °C. The

TABLE 1

Results of elemental analysis

Sample	M_1/M_2 molar ratio	Content, mass %			
		N	C	H	S
CeMo/Taunite	1/1	1.88	73.01	0.50	0.00
CuMo/Taunite	1/1	2.25	69.25	0.64	0.00
CeCu/Taunite	1/1	3.08	65.76	0.60	0.00
CeCu/Taunite	1/2	3.10	65.60	0.90	0.00
CeCu/Taunite	2/1	2.29	67.71	0.48	0.00
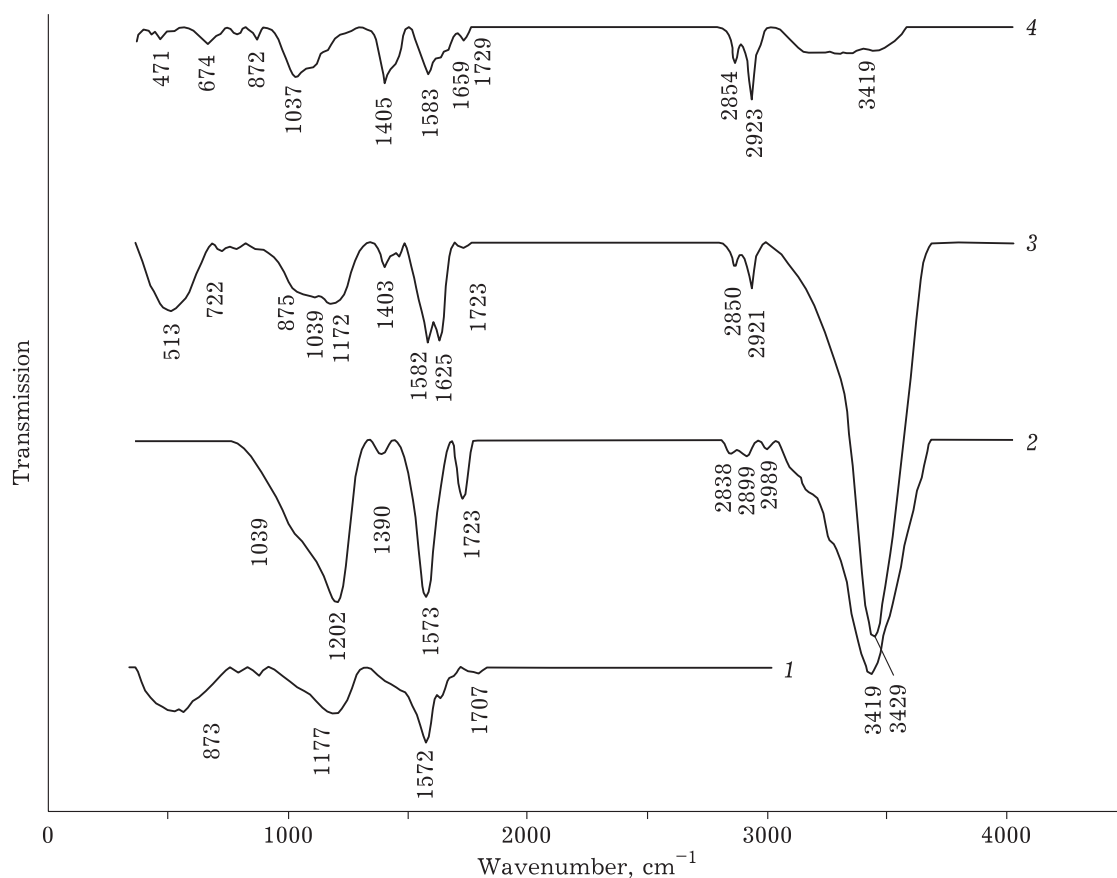
Fig. 2. FTIR spectra of samples: Taunite (*1*), Taunite-1 (*2*), CeCu/Taunite-1 (*3*), CeCu/Taunite (*4*).

gas evolved at the first and second stages is identified as water ($m/z = 18$) and ammonia ($m/z = 18$), while the second stage at a temperature of 100–290 °C is characterized by the emission of nitrogen oxide NO ($m/z = 30$). So, the composition of the gas phase shows that the presence of cerium (III) nitrate causes a decrease in the temperature of the transformation of $(NH_4)_6Mo_7O_{24} \cdot 4H_2O$ into oxide from 450 to <290 °C. Decomposition of ammonium heptamolybdate is likely to proceed with the formation of ammonium nitrate and molybdate ions, which are decomposed at heating to 150 °C. In addition, mass loss (7.73 %) without any thermal effect is observed within the temperature range from 290 to 800 °C and is accompanied by the evolution of CO_2 into the gas phase (see Fig. 3, *b*), which is the evidence of substantial degradation of the carbon matrix. Sublimation of molybdenum oxide may also promote mass loss at a temperature above 800 °C [9]. The difference between the expected mass loss (11.0 %) and the observed value ($Dm_\Sigma = 18.2$ %) is 7.2 % and may be assigned to the decomposition of the carbon matrix.

Thermal decomposition of supported salts $Ce(NO_3)_3 \cdot 6H_2O$ and $Cu(NO_3)_2 \cdot 3H_2O$ is a multistage process with $T_{DTG} = 80, 177, 233$ and 527 °C (Fig. 4, *a*). Three early peaks are due to the decomposition of Ce(III) and Cu(II) nitrates, namely dehydration (which includes two stages in the case of Ce(III)), the formation of anhydrous cerium nitrate, oxidation of Ce(III) by nitrate ion with the formation of CeO_2, the formation of intermediate compounds $Cu_2(OH)_3NO_3$ or $3Cu(NO_3)_2 \cdot Cu(OH)_2$, and the products CuO and Cu_2O at a temperature >310 °C. In the presence of CNT possessing reductive properties, endothermic peak due to the formation of Cu_2O shifts to lower temperature (875 °C → 525 °C) [9]. Dehydration starts at room temperature and finishes at ~290 °C. Before dehydration is over, the decomposition of the nitrate group starts. Between 130 and 290 °C, the evolution of H_2O ($m/z = 18$) and NO_2 ($m/z = 30$) is observed in the mass spectra. The temperature of the maximal emission of these gases decreases from 230 to 200 °C in comparison with bulk $Cu(NO_3)_3 \cdot 3H_2O$ [9]. According to MS data, CO_2 starts to pass into the gas phase even at a tem-
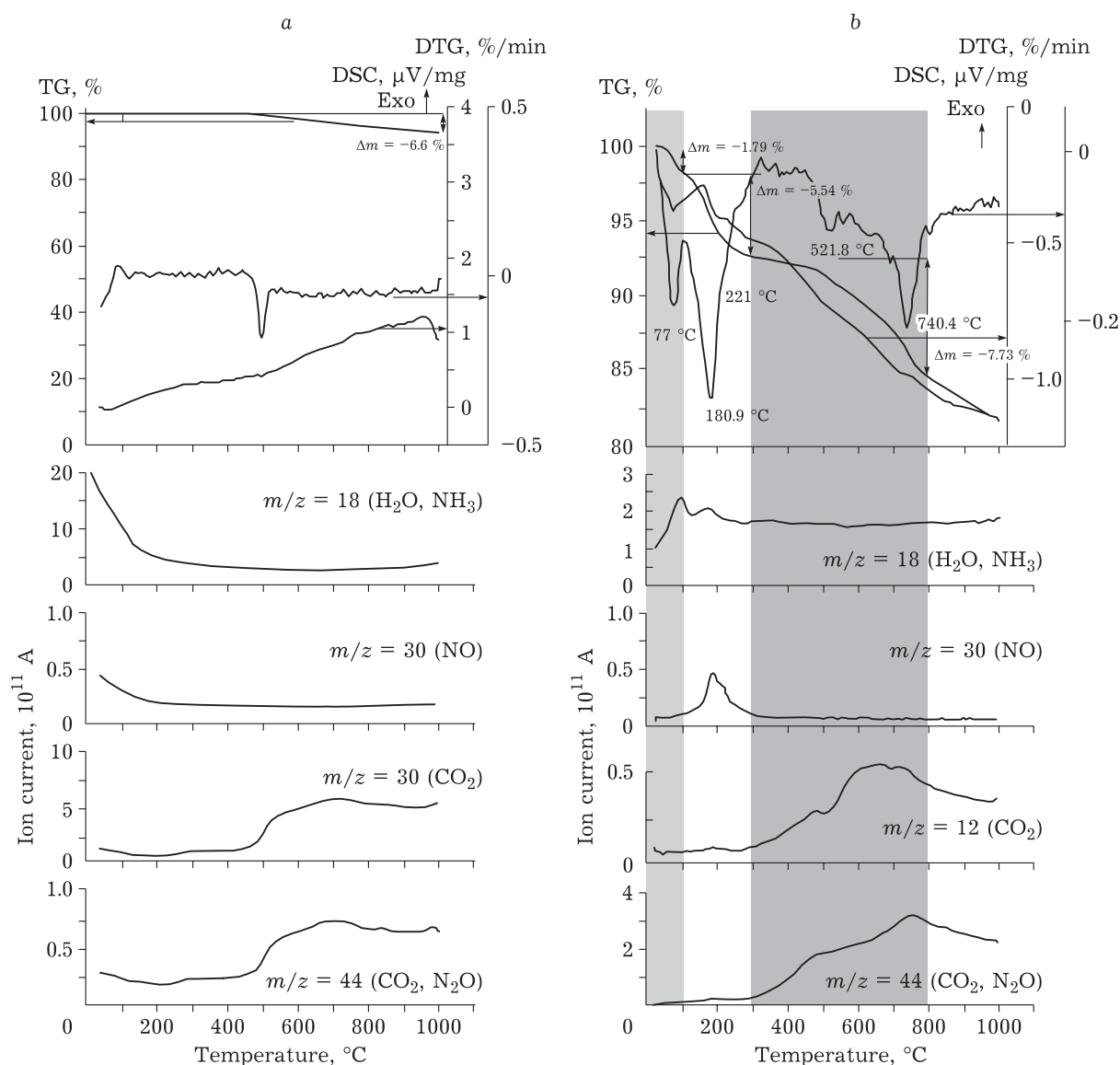
Fig. 3. TG, DTG, DSC and MS curves for samples: Taunite [9] (*a*) and CeMo/Taunite (Ce/Mo = 1 : 1) (*b*).

perature of 290 °C. Nevertheless, the loss of mass by the sample (Δm) at 580 °C is only 16.5 %, which is lower than the expected value of 22.7 % (−6.2 %). Lower Δm values may be explained by the partial decomposition of Cu(II) nitrate at the stage of drying in vacuum at 80 °C. The loss of mass by the sample at temperatures above 580 °C increases with an increase in $Cu(NO_3)_3 \cdot 3H_2O$ content (see Table 2). This is likely to be promoted by the presence of highly reactive nitrogen oxides entering oxidation-reduction reactions with carbon of the support. Indeed, according to the data of elemental analysis, nitrogen content in the CeCu/Taunite samples annealed at 600 °C in the inert atmosphere increases with an increase in Cu content. Mass loss after 290 °C is only 5.94 %,

which is substantially lower than the corresponding value for CeMo/Taunite sample (10.7 %).

Decomposition of supported salts $(NH_4)_6Mo_7O_{24} \cdot 4H_2O$ and $Cu(NO_3)_2 \cdot 3H_2O$ conserves the multistage nature of the decomposition of bulk samples [9] (see Fig. 4, *b*). Five steps are observed with T_{DTG} = 82, 132, 203, 350 and 525 °C. In this case, total mass loss (17.7 %) is somewhat larger than the expected value (15.7 %), which points to thermal destruction of the support. The difference between the observed and expected mass losses is 2 %, which is substantially smaller than for CeMo/Taunite sample (7.2 %). This fact agrees with the negative difference between the observed and expected Δm values at 580 °C for CeCu/Taunite sample and may be con-

TABLE 2

Data of thermal analysis and mass spectrometry for the decomposition of bulk and Taunite-supported precursors of the active component

Sample	Mass loss at different stages of decomposition (T_d range, °C)					Δm_Σ	Temperature of peaks at the DTG curve, °C (kind of thermal effect: exo/endo)					Gas products (T_e range, °C)
	Δm_1	Δm_2	Δm_3	Δm_4	Δm_5		T_1	T_2	T_3	T_4	T_5	
$Ce(NO_3)_3 \cdot 6H_2O$[a]	13.4 (25–130)	9.0 (130–230)	36.0 (230–400)	–	–	58.4	95 (endo)	195 (endo)	240 (endo)	–	–	H_2O (25–400) NO_x (200–400)
$(NH_4)_6Mo_7O_{24} \cdot 4H_2O$[a]	4.8 (25–110)	4.3 (110–160)	2.0 (160–250)	5.6 (250–350)	1.4 (350–500)	18.1	95 (endo)	120 (endo)	200 (экзо)	295 (endo)	380 (endo)	H_2O (25–500) NH_3 (25–500) NO_x (250–500)
$Cu(NO_3)_2 \cdot 3H_2O$[a]	37.6 (25–165)	16.1 (165–245)	9.8 (245–300)	3.1 (300–860)	4.3 (860–1000)	70.9	120 (endo)	200 (endo)	265 (endo)	875 (endo)	–	H_2O (25–300) NO_x (120–400)
CeMo/Taunite	1.79 (25–100)	5.73 (100–290)	7.54 (290–800)	3.16 (800–1000)	–	18.22	181 (endo)	521 (endo)	740 (endo)	–	–	H_2O (25–290) NO (100–290) CO_2 (290–900) CO_2, N_2O (290–900)
CeCu/Taunite Ce/Cu = 1/2	3.06 (25–130)	4.46 (130–200)	5.46 (200–290)	2.04 (290–580)	6.58 (580–1000)	21.6	80 (endo)	176 (endo)	232 (endo)	527 (endo)	–	H_2O (25–290) NO (130–290) CO_2 (290–900) CO_2, N_2O (290–900)
CeCu/Taunite Ce/Cu = 1/1	4.32 (25–130)	4.04 (130–200)	5.72 (200–290)	2.4 (290–580)	3.54 (580–1000)	20.02	80 (endo)	173 (endo)	227 (endo)	522 (endo)	–	H_2O (25–290) NO (130–290) CO_2 (290–900) CO_2, N_2O (290–900)
CeCu/Taunite Ce/Cu = 2/1	3.48 (25–130)	3.2 (130–200)	3.99 (200–290)	2.33 (290–580)	2.63 (580–1000)	15.63	79 (endo)	101 (endo)	185 (endo)	242 (endo)	521 (endo)	H_2O (25–230) NO (100–300) CO_2 (290–900) CO_2, N_2O (290–900)
CuMo/Taunite	5.45 (25–215)	1.99 (215–320)	8.32 (320–800)	1.91 (800–1000)	–	17.67	132 (endo)	235 (endo)	524 (endo)	706 (endo)	–	H_2O (25–320) NO (100–320) CO_2 (215–900) CO_2, N_2O (215–900)

Note. 1. Δm_i is mass loss corresponding to different stages of decomposition, %; Δm_Σ is total mass loss at 1000 °C, %; T_d is decomposition temperature., °C; T_e is temperature of the evolution of gas products, °C. 2. Dash means the absence of peak on the curves of thermal analysis.

[a] According to the data reported in [9].
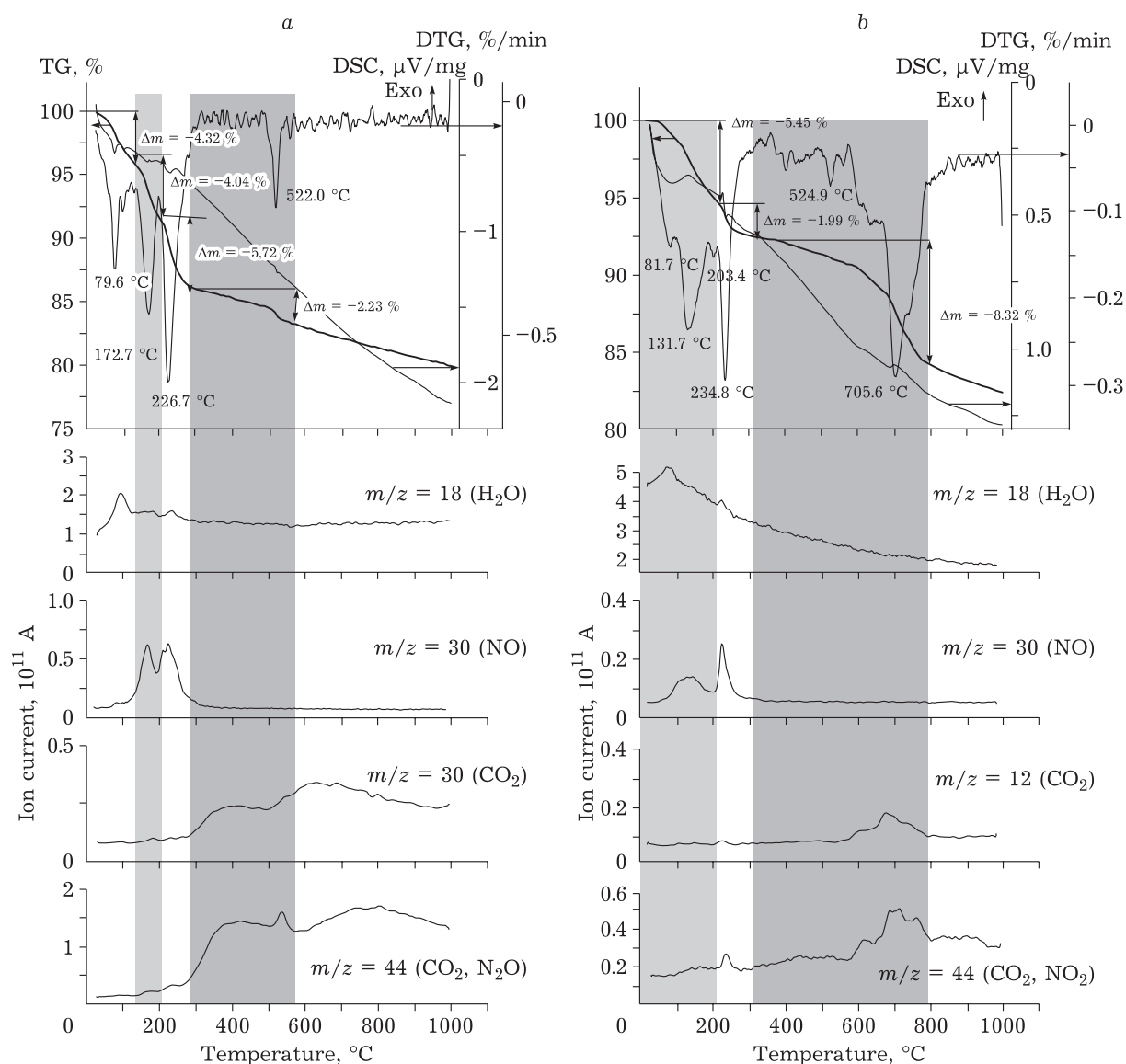
Fig. 4. TG, DTG, DSC and MS curves for samples: CeCu/Taunite (Ce/Cu = 1 : 1) (*a*) and CuMo/Taunite (Cu/Mo = 1 : 1) (*b*).
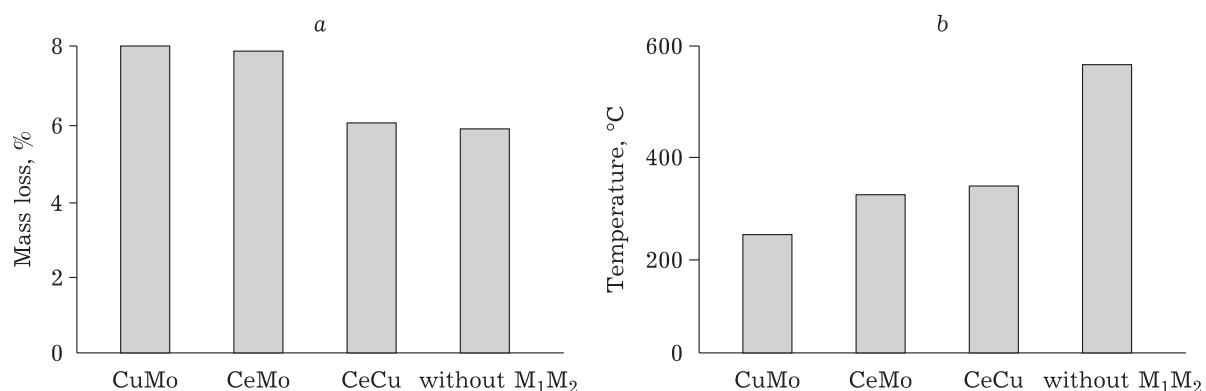
Fig. 5. Effect of precursor nature on the oxidation/decomposition of the support during thermal treatment (in N_2) of dried $M_1M_2O_x$/Taunite samples: mass loss (*a*) and the temperature of the start of CO_2 evolution (*b*).

nected with the partial decomposition of Cu(II) precursor at the stage of drying. According to MS data, the evolution of H_2O ($m/z = 18$) and NH_3 ($m/z = 18$) occurs within the range 25–320 °C. Between 100 and 320 °C, mass spectra reveal the evolution of NO_2 ($m/z = 30$); CO_2 ($m/z = 44$, $m/z = 12$) starts to evolve at 215 °C and has two maxima at 230 and 700 °C. The maximal mass loss (8.54 %) is observed for this sample at a temperature within 320–800 °C without taking into account possible sublimation of MoO_3.

So, the introduction of the salt causes a decrease in the stability of carbon support to thermal degradation; its extent depends on the type of metal precursor used. The decomposition of the support involves the reactions of complete oxidation of the carbon support by gases evolves during the decomposition of metal salts. Essential factors are the temperature of decomposition of metal compounds, the composition of gases, and the catalytic activity of metals in the oxidation of organic substrates. The stability of CNT against thermal destruction increases in the sequence of metal cations: CuMo < CeMo < CeCu < without M_1M_2 (Fig. 5, *a*). Among the studied metals, the highest reactivity was that of Cu and Mo. In the presence of these metals, the lowest temperatures of the start of CNT matrix degradation were observed (see Fig. 5, *b*).

CONCLUSION

For the purpose of developing new catalysts based on CNT with supported bimetal oxide nanoparticles for the oxidative transformations of sulphur-containing compounds, a set of samples with the composition $M_1M_2O_x$/Taunite was prepared by means of incipient wetness impregnation with variations of the type of active metal (M_1M_2 = CeMo, CuMo, CeCu). The effect of the nature of active component precursors on the functional composition of the surface of the support and its thermal stability was studied by means of IR spectroscopy and thermal analysis in combination with mass spectrometry. It was demonstrated by means of IR Fourier spectroscopy that the oxidation of Taunite by concentrated nitric acid leads to the formation of oxygen-containing groups. The content of oxygen-containing groups decreases for the support decorated with bimetal oxides. The stability of the CNT support to thermal decomposition increases in the sequence:

CuMo < CeMo < CeCu < without M_1M_2. The nitrates of Ce(III) and Cu(II) may be used as the precursors of the active component for the synthesis of a promising catalyst based on CNT Taunite with supported bimetal oxide nanoparticles.

REFERENCES

1 Jiang W., Zheng D., Xun S., Qin Y., Lu Q., Zhu W., Li H., Polyoxometalate-based ionic liquid supported on graphite carbon induced solvent-free ultra-deep oxidative desulfurization of model fuels, *Fuel*, 2017, Vol. 190, P. 1–9.

2 Gao Y., Gao R., Zhang G., Zheng Y., Zhao J., Oxidative desulfurization of model fuel in the presence of molecular oxygen over polyoxometalate based catalysts supported on carbon nanotubes, *Fuel*, 2018, Vol. 224, P. 261–270.

3 Zhang W., Zhang H., Xiao J., Zhao Z., Yu M., Li Z., Carbon nanotube catalysts for oxidative desulfurization of a model diesel fuel using molecular oxygen, *Green Chem.*, 2014, Vol. 16, P. 211–220.

4 Ismagilov Z. R., Yashnik S. A., Shikina N. V., Matus E. V., Efimova O. S., Popova A. N., Nikitin A. P., Effect of acid treatment on the functionalization of surface, structural and textural properties of carbon nanotubes taunit, *Eurasian Chem. J.*, 2019, Vol. 21, P. 291–302.

5 Saleh T. A., Al-Hammadi S.A., Tanimu A., Alhooshani K., Ultra-deep adsorptive desulfurization of fuels on cobalt and molybdenum nanoparticles loaded on activated carbon derived from waste rubber, *J. Colloid Interface Sci,.* 2018, Vol. 513, P. 779–787.

6 Danmaliki G. I., Saleh T. A., Influence of conversion parameters of waste tires to activated carbon on adsorption of dibenzothiophene from model fuels, *J. Clean. Prod.*, 2016, Vol. 117, P. 50–55. https://doi.org/10.1016/j.jclepro.2016.01.026.

7 Wu P., Zhu W., Dai B., Chao Y., Li C., Li H., Zhang M., Jiang W., Li H., Copper nanoparticles advance electron mobility of graphene-like boron nitride for enhanced aerobic oxidative desulfurization, *Chem. Eng. J.*, 2016, Vol. 301, P. 123–131.

8 Wu Z., Cai X., Yang Z., Effects of functional group modification on the thermal properties of nano-carbon clusters, *J. Nanoparticle Res.*, 2015, Vol. 17, P. 1–8.

9 Matus E. V., Khitsova L. M., Efimova O. S., Yashnik S. A., Shikina N. V., Ismagilov Z. R., Preparation of carbon nanotubes with supported metal oxide nanoparticles: Effect of metal precursor on thermal decomposition behavior of the materials, *Eurasian Chem. J.*, 2019, Vol. 21, P. 303–316.

10 Prasad V. V. D. N., Jeong K. E., Chae H. J., Kim C. U., Jeong S. Y., Oxidative desulfurization of 4,6-dimethyl

dibenzothiophene and light cycle oil over supported molybdenum oxide catalysts, *Catal. Commun.*, 2008, Vol. 9, P. 1966−1969.

11 Cao Y., Wang H., Ding R., Wang L., Liu Z., Lv B., Highly efficient oxidative desulfurization of dibenzothiophene using Ni modified MoO_3 catalyst, *Appl. Catal. A Gen.*, 2020, Vol. 589, Article 117308.

12 Hasannia S., Kazemeini M., Rashidi A., Seif A., The oxidative desulfurization process performed upon a model fuel utilizing modified molybdenum based nanocatalysts: Experimental and density functional theory investigations under optimally prepared and operated conditions, *Appl. Surf. Science,* 2020, Vol. 527, Article 146798.

13 Wang X., Zhang D., Li Y., Tang D., Xiao Y., Liua Y., Huo Q., Self-doped Ce^{3+} enhanced CeO_2 host matrix for energy transfer from Ce^{3+} to Tb^{3+}, *RSC Adv.,* 2013, Issue 11, P. 3623−3630.

14 Zhang J., Bai X., Li X., Wang A., Ma X., Preparation of MoO_3-CeO_2-SiO_2 oxidative desulfurization catalysts by a sol-gel procedure, *Chin. J. Catal.,* 2009, Vol. 30, Issue 10, P. 1017−1021.

15 Shi Y., Liu G., Zhang B., Zhang X., Oxidation of refractory sulfur compounds with molecular oxygen over a Ce-Mo-O catalyst, *Green Chem.,* 2016, Vol. 18, Issue 19, P. 5273−5279.

16 Ismagilov Z. R., Shalagina A. E., Podyacheva O. Y., Ischenko A. V., Kibis L. S., Boronin A. I., Chesalov Y. A., Kochubey D. I., Romanenko A. I., Anikeeva O. B., Buryakov T. I., Tkachev E. N., Structure and electrical conductivity of nitrogen-doped carbon nanofibers, *Carbon,* 2009, Vol. 47, P. 1922−1929.

17 Socrates G., Infrared and Raman Characteristic Group Frequencies: Tables and Charts, 3rd Ed., Hoboken, NJ: John Wiley & Sons Ltd. 2001. 366 p.

18 Ros T. G., Van Dillen A. J., Geus J. W., Koningsberger D. C., Surface structure of untreated parallel and fishbone carbon nanofibres: An infrared study, *ChemPhysChem.,* 2002, Vol. 3, P. 209−214.

19 Ros T. G., Van Dillen A. J., Geus J. W., Koningsberger D. C., Surface oxidation of carbon nanofibres, *Chem. A Eur. J.,* 2002, Vol. 8, P. 1151−1162.

20 Stobinski L., Lesiak B., Кцvйr L., Tyth J., Biniak S., Trykowski G., Judek J., Multiwall carbon nanotubes purification and oxidation by nitric acid studied by the FTIR and electron spectroscopy methods, *J. Alloys Compd.,* 2010, Vol. 501, P. 77−84.

21 Alshabib M., Oluwadamilare M. A., Tanimu A., Abdulazeez I., Alhooshani K., Ganiyu S. A., Experimental and DFT investigation of ceria-nanocomposite decorated AC derived from groundnut shell for efficient removal of methyleneblue from wastewater effluent, *Appl. Surf. Sci.,* 2021, Vol. 536, Article 147749.

22 Seguin L., Figlarz M., Cavagnat R., Lassиgues J. C., Infrared and Raman spectra of MoO3 molybdenum trioxides and $MoO_3 \cdot x H_2O$ molybdenum trioxide hydrates, *Spectrochim. Acta Part A Mol. Biomol. Spectrosc.,* 1995, Vol. 51, P. 1323−1344.

23 Zawadzki M., Preparation and characterization of ceria nanoparticles by microwave-assisted solvothermal process, *J. Alloys Compd.,* 2008, Vol. 454, P. 347−351.

24 Serin N., Serin T., Horzum Ş., Çelik Y., Annealing effects on the properties of copper oxide thin films prepared by chemical deposition, *Semicond. Sci. Technol.,* 2005, Vol. 20, P. 398−401.